Optical coherence tomography in pulmonary imaging: Feasibility study

Woonggyu Jung[1,3], Jun Zhang[1], Petra Wilder-Smith[1], Minaaraghi Reza[1,2], Matt Brenner[1,2], Yongjin Shin[1,5], J. Stuart Nelson[1,3,4], Zhongping Chen[1,3]

[1]Beckman Laser Institute, University of California, Irvine,
[2]Pulmonary Division, UCI Medical Center,
[3]Department of Biomedical Engineering, University of California, Irvine
[4]Department of Surgery, UCI Medical Center,
[5]Department of Physics, Chosun University, Korea

ABSTRACT

We suggest that Optical coherence tomography (OCT) is a potential imaging modality capable of assisting diagnosis in pulmonary medicines. OCT can provide extremely high resolution imaging and be performed with flexible fiber-optic bronchoscopy with small diameter endoscopic probes. In this study, animal models of trachea, and lung surface were to investigate utility of OCT in pulmonary. Normal, malignant, and infectious disease animal model samples measured by OCT were compared to standard histologic H&E light microscopic imaging of the same sites.

1. BACKGROUND

Lung cancer is the leading cause of cancer death in men and women in the United States. To date, various medical technologies such as ultrasound, CT and MRI have been used as diagnostic tools, but high-resolution and minimally invasive techniques for imaging in-vivo tissue structure are currently unavailable. Improved methods are essential for more accurate diagnosis and staging of many diseases including cancer and infectious pulmonary conditions.

Optical coherence tomography (OCT) is an evolving imaging modality[1, 2] used to obtain high-resolution, high-speed, non-invasive or minimally invasive endoscopic imaging of biological tissues. Frequently, OCT is compared with ultrasound because both technologies employ back-scattered signals reflected from different layers within the tissue to reconstruct structural images. OCT is based on the detection of light waves rather than sound, which enables resolution in the range of 2-10 μm with near real-time image acquisition.

The most extensive clinical use of OCT has been in the field of ophthalmology. The eye provides a uniquely suitable medium for OCT imaging due to its transparent nature, minimal scattering and excellent light penetration[3]. The ability of OCT to be incorporated into flexible fiberoptic probes has broadened the range of endoscopic imaging to gastroenterology[4], cardiology[5], and urology[6]. Fiberoptic capabilities enable *in-situ* imaging of virtually any organ accessible by a catheter or endoscope. In pulmonary medicine, endoscopic tools such as flexible bronchoscopy are a mainstay of diagnostics and therapeutics for endobronchial diseases including inflammatory conditions, malignancy and infections.

Coherence Domain Optical Methods and Optical Coherence Tomography in Biomedicine VIII, edited by Valery V. Tuchin, Joseph A. Izatt, James G. Fujimoto, Proc. of SPIE Vol. 5316 (SPIE, Bellingham, WA, 2004) · 1605-7422/04/$15 · doi: 10.1117/12.529824

The purpose of this study was to evaluate the feasibility of OCT for high resolution imaging in pulmonary. Animal models of trachea and lung were imaged by OCT. Our study also focused on detection of cancer with rabbit lung and hamster cheek pouch. However, the results should be directly applicable to other cancer detection priority areas such as breast, cervical, colon, prostate, and skin.

2. METHODS

2.1 Model Preparation

In this study, images from normal and diseased septic and malignant animal models, rabbit, hamster were obtained. For the control groups, animals were sacrificed according to ARC approved protocols, and their pulmonary tissue including tracheas and lungs were removed and maintained in isotonic saline until imaged.

Septic detection feasibility group animals were treated with various doses of S. Pneumoniae inoculated into the animal's airways through a sterile pediatric suction catheter. Animals developed pneumonia and sepsis following the inoculation. Malignant cancer model animals underwent thoracoscopic injection of sarcoma cells (10 ×106 cells) into the rabbit lung parenchyma and hamster cheek pouch. Cancer injected animals were sacrificed 2-3 weeks after injection.

Tracheas were cut and opened longitudinally along their musculofibrous membranes and divided into approximately 1cm × 2cm sections. The imaging sites for OCT were marked with wedge incisions. Samples were then fixed in formalin and prepared for standard H&E sectioned histologic slides of the corresponding regions. The cheek pouches were inverted, held in place with a fixation device, and imaged. After imaging, hamsters were euthanized and the specimens excised for histologic preparation.

2.2 Imaging

A schematic of the OCT system is shown in Fig. 1. A low-coherence length light source that delivered an output power of 10 mW at a central wavelength of 1310 nm with a bandwidth of 70 nm is coupled into a fiber based Michelson interferometer. Scanning devices directed towards the tissue are in the sampling arm of the interferometer and a rapid-scanning optical delay line (RSOD) is in the reference arm. A visible aiming beam (633 nm) was used to locate the exact position and path on the sample.

Two types of imaging delivery devices were employed, both used linear scanning[7]. One was a moving stage line system with an objective lens and collimator, the other a linear scanning flexible fiberoptic catheter for endoscopic OCT which includes a GRIN lens and prism[2,8]. The catheter consisted of main three components: single mode fiber, GRIN lens and micro prism. A single mode fiber with a core diameter of 9 μm guides the light through the center of the endoscopic probe. The distal end was comprised of a 0.7 mm diameter, 0.2725 pitch GRIN lens, and a 0.5 mm right angle micro prism. The outer diameter of the endoscopic probe was a 2 mm transparent window. The focal length of this probe was 2.5 mm with a 45 μm spot size. This probe was used for linear scanning by connecting the proximal fiber to the scanning stage.

In the reference arm, a RSOD was used that employs a grating to control the phase and

group delays separately so that no phase modulation was generated when the group delay was scanned[9, 10]. The phase modulation was generated through an electro-optic phase modulator that produces a carrier frequency. The axial line scanning rate was 400 Hz and the modulation frequency was 500 kHz.

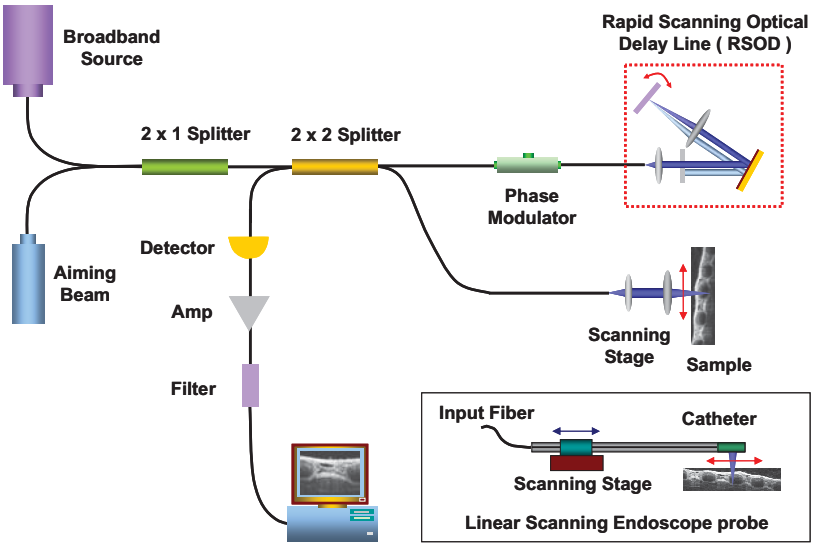

Figure. 1. Schematic of the OCT system. Two beam delivery devices were used: a lens system and a flexible fiberoptic catheter with a GRIN lens and prism were used in the sample arm of interferometer. Both systems were used to perform linear scanning: RSOD, rapid scanning optical delay line.

Reflected beams from the two arms are recombined in the interferometer and detected with a photodetector. Interference signals are observed only when the optical path length difference of the two interferometer arms matched within the source coherence path length. The detected optical interference fringes intensity signals are filtered at the carrier frequency and resultant signals are displayed as 2D images with 10 μm axial resolution after signal processing.

3. Results

Fig. 2 shows a representative OCT image and corresponding histology of normal and abnormal rabbit trachea. The OCT images corresponded very closely to the histological light microscopic photograph. Epithelium, mucosa, cartilage are clearly differentiated as well as a number of glandular tissues by both OCT (left) and histology (right). The similarity between the OCT image and the corresponding standard histologic image is readily evident. In contrast to normal trachea, mucosal and submucosal edema is noted in the inflamed trachea by OCT (C) and H&E (D). The septic specimens showed marked edema and swelling of the submucosal region, with glandular structures visualized. Inflamed tracheas were easily distinguished from normal specimens due to these submucosal changes. Some of the edema was not evident in the histologic sections due to desiccation of the tissue samples during preparation.

Fig. 3 presents *in-vitro* endoscopic images of inflamed trachea obtained from an intubated septic rabbit acquired through an endotracheal tube. Epithelial, mucosal and submucosal

structures are seen.

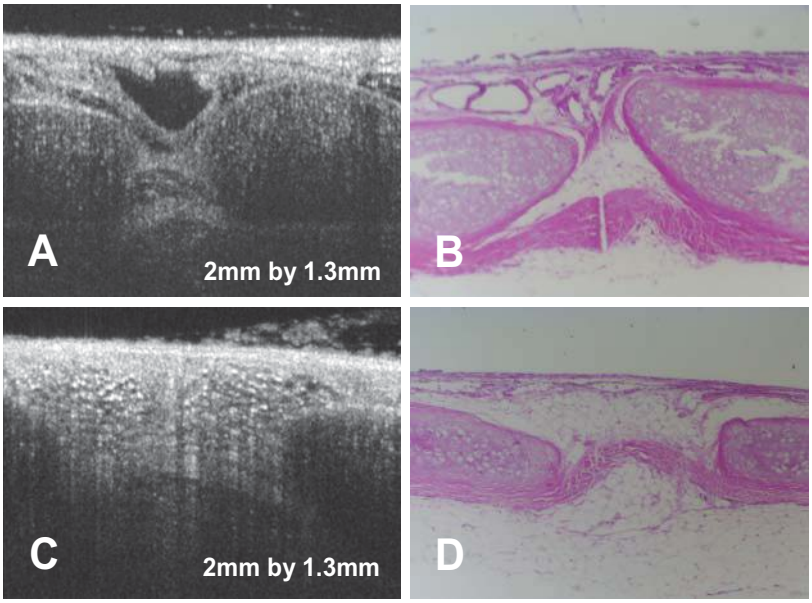

Figure. 2. Comparison between OCT imaging and H&E section of rabbit trachea: Top, normal rabbit trachea by OCT (A) and H&E (B); Bottom, septic rabbit trachea which is shown mucosal and submucosal edema by OCT (C) and H&E (D).

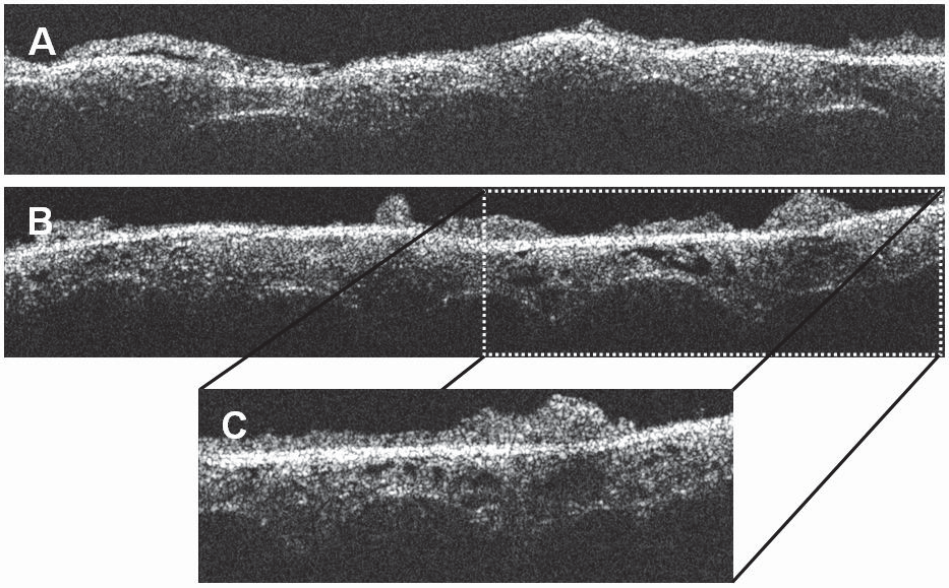

Figure. 3. *In-vitro* flexible fiberoptic endoscopic OCT image of rabbit trachea: Fig. A, B were obtained from the septic rabbit trachea in different disease stages (8 × 1.3mm, 10μm/pixel); C, higher magnification view of Fig. 3 (B). The size of OCT image is 4 × 1.3mm with 10μm/pixel. Similar to Fig. 2, the septic tracheal specimens showed marked edema and swelling of the submucosal region, with observed glandular structures using the flexible fiberoptic probe to obtain the images.

Fig. 3 (A), (B) were obtained in the inflamed trachea IN different stages of infection and Fig. 3 (C) shows higher magnification view of Fig. 3 (B). Similar to Fig. 2, the inflamed tracheal specimens showed marked edema and swelling of the submucosal region, with glandular structures. Fig. 3 shows the ability to obtain high-resolution OCT images was under technically challenging conditions such as intubation. Similar structural information was previously obtained with the stage system, but image contrast is lower because the image was acquired through the wall of an endotracheal tube, leading to boundary loss from the tube walls. Another cause of lower contrast with the endoscopic OCT system is that the image was captured in a region beyond the fixed lens focal point because of the added thickness of the endotracheal tube. However, despite the technically challenging conditions under which this image was acquired, the endoscopic OCT image still has adequate resolution to distinguish structures and reveal edema formation in the abnormal trachea similar to those seen in Fig. 2. In clinical practice, one would not image through the wall of the endotracheal tubes, but would pass the probe through the bronchoscope and image the mucosa directly.

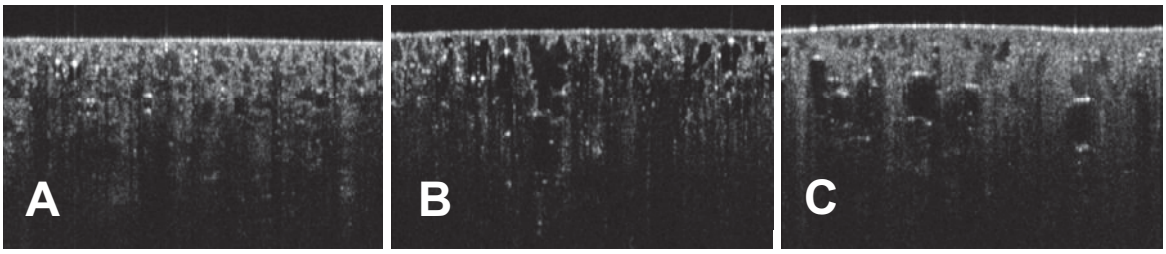

Figure 4. Rabbit lung OCT images (2 × 1.3mm, 10μm/pixel): A, normal rabbit lung showing pleural surface (top surface), as well as alveolar structures below surface; B, normal rabbit lung instilled with saline. Alveolar structures appear more clearly defined, and somewhat larger due to the liquid instillation; C, normal lung instilled with formalin. Again, pleural and alveolar structures can be seen.

Fig. 4 demonstrates OCT imaging of normal rabbit lung. At the upper portion of Fig. 4 (A), the pleural surface can be seen. The pleural surface in rabbit lung is a fine smooth cellular layer. Below the pleural surface, and alveolar spaces can be visualized. Fig. 4 (B) in the center shows the same rabbit lung instilled with normal saline to 20 cm of water pressure. The lung architecture is now better visualized, and the alveoli appear somewhat larger with the fluid filling. The pleural surface is again well visualized in the upper portion of the Fig. 4 (B). In Fig. 4 (C), formalin preserved normal rabbit lung imaging with OCT is shown. Again, the pleural surface and alveolar structures can be seen.

Fig. 5 shows the comparison between OCT lung images and standard H&E histology slide of normal rabbit lung. In Fig. 5 (A), the pleural surface, and alveolar structures are clearly seen. In the H&E histological specimen of normal rabbit lung, the similarity between the pleural and alveolar structural imaging is clearly evident.

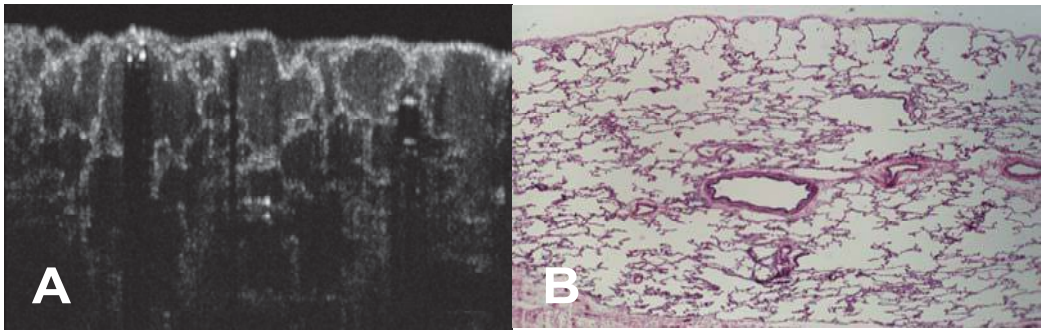

Figure 5. Rabbit lung OCT (2 × 1.3mm, 10μm/pixel) compared to histology: A, rabbit lung OCT image showing pleura (upper surface), and alveoli below the pleural surface; B, standard histologic picture of similar area of rabbit lung showing pleural surface and sub-pleural alveoli.

The images in Fig. 6 compare OCT and H&E picture of a fungiform malignant cancer. The epithelium is folded, as are the mucosa and basement membrane. The basement membrane is no longer intact due to the invasion of the malignant cells into the connective tissue below. The cancer tissue appears darker in the OCT image in part because it contains more blood than healthy tissue. The OCT system used in these studies employs a 1300 nm light source. At this wavelength, light absorption by blood is considerable, giving rise to the darker appearance of the malignant tissue.

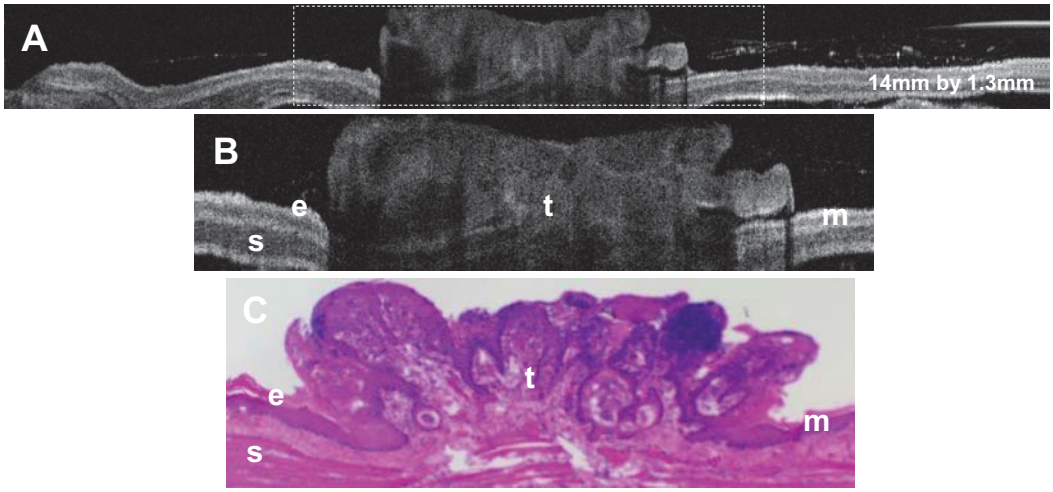

Figure 6. *In-vivo* OCT image and H&E section of hamster cheek pouch with fungiform cancer: A, a 14 mm segment of hamster cheek pouch obtained by OCT; B is the higher magnification views of Fig. 6 (A). The size of OCT images shown is 6 × 1.3mm with 10 μm/pixel display resolution; C shows H&E section corresponding with Fig. 6 (B): e, squamous epithelium; m, mucosa; s, submucosa, t, fungiform malignant tissue.

Fig. 7 shows OCT imaging and histologic pictures of the malignant (VX2 Sarcoma cell) lung cancer. Fig. 7 (A) shows lung parenchymal surface with multiple hematogenously disseminated small lung malignant tumor nodules. These cancer nodules range in size from approximately 50-400 μm in diameter. In Fig. 7 (B), a low magnification image of rabbit lung with hematogenous cancer nodules is shown. In Fig. 7 (C), a higher magnification histologic image of this same cancer confirms the presence of malignancy with obvious sarcoma cells containing large, irregular dark staining nuclei and disruption of normal lung architecture.

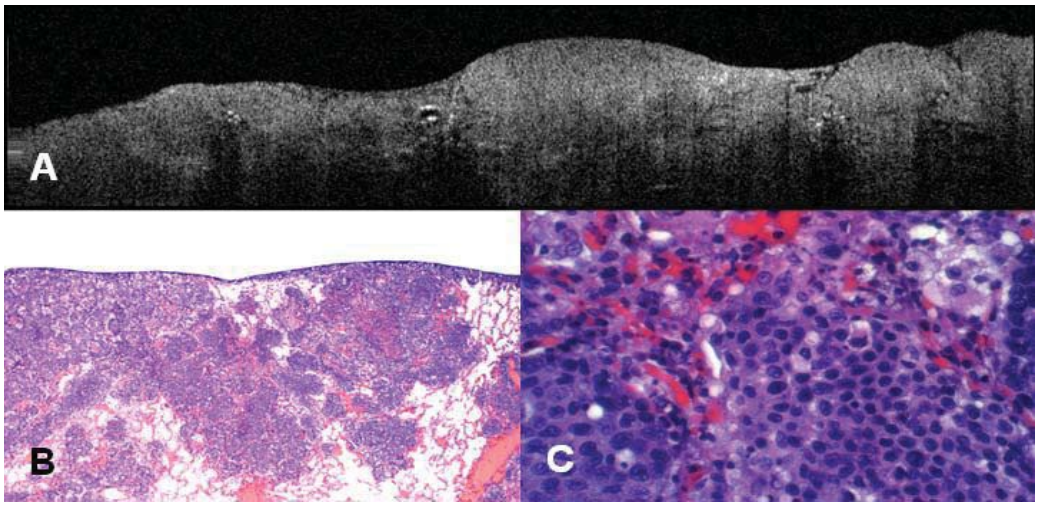

Figure 7. Rabbit malignant lung cancer (VX2 sarcoma) OCT and histology: A, rabbit lung OCT image (6 × 1.3 mm, 10 μm/pixel) showing sub-pleural malignant cancer; B, standard histologic image of a similar area of rabbit lung cancer showing malignant tumor; C, higher power magnification of histologic section of the malignant cancer.

4. CONCLUSIONS

This study documents that OCT is a potential imaging modality for pulmonary regions capable of visualizing microstructural changes with disease. Normal, malignant, and infectious disease animal model samples were imaged by OCT which was able to distinguish many histologic features, usually requiring biopsy. In the trachea, notable differences between normal and septic model were detected by OCT. We have also successfully demonstrated the use of OCT for cancer detection and diagnosis of malignancy.

ACKNOWLEDGEMENTS

The authors would like to thank David S. Mukai, and Naglaa E. Abbadi for expertise and technical support in histological evaluation. We also thank Drs. Ron Walton, Andre Yershov, and Brian Jordan at the Institute of Surgical Research, San Antonio for the septic tracheal specimens.

This work was supported by research grants awarded from the National Science Foundation (BES-86924), California Tobacco Related Disease Research Program #6RT-0158, and National Institutes of Health (EB-002SS, EB-00293, EB-002495, NCI-91717, RR-01192,

AR47SS1). Philip Morris External Research Program PMUSA-32598, Institute support from the Air Force Office of Scientific Research (F49620-00-1-0371), and the Beckman Laser Institute Endowment is also gratefully acknowledged.

REFERENCES

[1] D. Huang , E. A. Swanson, C. P. Lin, J. S. Schuman, W. G. Stinson, W. Chang W, M. R. Hee, T. Flotte, K. Gregory, C.A. Puliafito, J. G. Fujimoto, "Optical coherence tomography," *Science*, vol. 254, pp. 1178-1181, 1991.

[2] Tearney GJ, Brezinski ME, Bouma BE, Boppart SA, Pitris C, Southern JF, Fusimoto JG, "In vivo endoscopic optical biopsy with optical coherence tomography", *Science*, Vol. 276, pp. 2037-2039, 1997.

[3] M. R. Hee, J. A. Izatt, E. A. Swanson *et al*., "Optical coherence tomography of the human retina", *Arch Ophthalmol*, Vol. 113, pp. 325-32, 1995.

[4] Kenji Kobayashi, Joseph A. Izatt, Manish D. Kulkarni, Joseph Willis, Michael V. Sivak Jr., "High-resolution cross-sectional imaging of the gastrointestinal tract using optical coherence tomography: preliminary results", *Gastrointest Endosc*, Vol. 47, No. 6, pp. 515-23, 1998.

[5] Yelbuz TM, Choma MA, Thrane L, Kirby ML, Izatt JA, "Optical coherence tomography: a new high-resolution imaging technology to study cardiac development in chick embryos", *Circulation*, Vol. 106, No.22, pp. 2771-4, 2002.

[6] Tearney, G. J., Brezinski, M. E., Southern, J. F., Bouma, B. E., Boppart, S. A., & Fujimoto, J. G., "Optical biopsy in human urologic tissue using optical coherence tomography", *Journal of Urology*, 157, 1915-1919, 1997.

[7] B. E. Bouma, G. J. Tearney, "Power-efficientnonreciprocal interferometer and linear-scanning fiber-opticcatheter for optical coherence tomography", *Opt. Lett*, Vol. 24, No. 8, pp. 531-533, 1999.

[8] G. J. Tearney, S. A. Boppart, B. E. Bouma, M. E. Brezinski, N. J. Weissman, J. F. Southern, J. G. Fujimoto, "Scanning single-mode fiber optic catheter-endoscope for optical coherence tomography", *Opt. Lett*, Vol. 21, No. 7, pp. 543-545, 1996.

[9] G. J. Tearney, B. E. Bouma, F. G. Fujimoto, "High-speed phase- and group-delay scanning with a grating-based phase control delay line," *Opt. Lett*., Vol. 22, pp. 1811-1813, 1997.

[10] A. M. Rollins, M. D. Kulkarnis, S. Yazdanfar, R. Ung-arunyawee, J. A. Izatt, "In vivo video rate optical coherence tomography," *Opt. Express*., Vol. 3, pp. 219-229, 1998.